Absolute Raman matrix elements of graphene and graphite

Rohit Narula,[1,2] Robert Panknin,[2] and Stephanie Reich[2]
[1]*Department of Materials Science and Engineering, The Massachusetts Institute of Technology, Cambridge, Massachusetts 02139, USA*
[2]*Fachbereich Physik, Freie Universitat Berlin, Arnimallee 14, Berlin 14195, Germany*
(Received 25 February 2010; revised manuscript received 4 June 2010; published 20 July 2010)

Using sample substitution [Grimsditch *et al.*, J. Raman Spectrosc. **10**, 77 (1981)] we deconvolve the highly wavelength-dependent response of the spectrometer from the Raman spectra of graphene suspended on an SiO_2-Si substrate and graphite for the *D* and *G* modes in the visible range. We derive a model that considers graphene suspended on an arbitrary stratified medium while sidestepping its problematic ascription as an object of finite thickness and calculate the absolute Raman response of graphene (and graphite) via its explicitly frequency-independent Raman matrix element [Falicov and Martin, *Light Scattering in Solids I: Introductory Concepts* (Springer-Verlag, Berlin, 1983), p. 1083] $|K'_{2f,10}|^2$ vs laser frequency. For both graphene and graphite the $|K'_{2f,10}|^2$ per graphene layer vs laser frequency rises rapidly for the *G* mode and less so for the *D* mode over the visible range. Although we find a dispersion of the *D* mode position with laser frequency for both graphene and graphite of 41 cm^{-1}/eV and 35 cm^{-1}/eV, respectively, in good agreement with Narula and Reich [Phys. Rev. B **78**, 165422 (2008)] assuming constant matrix elements, the observed intensity dependence is in disagreement. Finally, we show the sensitivity of our calculation to the variation in thickness of the underlying SiO_2 layer for graphene. Our findings shall serve as an experimental verification of the behavior of the relevant matrix elements in graphene and its allotropes that may be calculated theoretically in the future.

DOI: 10.1103/PhysRevB.82.045418 PACS number(s): 78.30.Fs, 63.22.Rc, 81.05.U−

I. INTRODUCTION

As a material system graphene[1] has enjoyed an unabated surge in popularity as a research subject owing to its novel physics, promise as an interconnect material and sensing abilities.[2] The key to understanding the optical properties of graphene and its allotropes lies in knowing the behavior of the matrix elements and resonant denominators that constitute the processes underlying such phenomena. Optical spectroscopies provide access to different combinations of matrix elements. For example, the Raman *G* mode in graphene and graphite at ~ 1600 cm^{-1} arises from the interplay of the electron-radiation and electron-phonon interaction matrix elements. Whereas the *D* mode, a signature of structural disorder and present at ~ 1350 cm^{-1} in addition involves the electron-defect scattering matrix element. However, the measured spectra are obscured by the response of the spectrometer and the influence of the underlying substrate via electric field enhancement that needs to be deconvolved to obtain the absolute Raman response of the material. Recently the so-called Raman matrix element[3,4] $K_{2f,10}$ corresponding to the *D* mode for graphene and graphite based on the double-resonance model of Thomsen and Reich[5,6] has been calculated over the entire two-dimensional Brillouin zone of graphene under the assumptions of constant matrix elements and a single value of the broadening parameter for each transition.[7] Although the literature is rife with studies of the Raman spectra of different variants of sp^2 carbon detailing their respective peak structure with and without additions such as functional groups or defects,[8,9] to our knowledge the absolute Raman response of the *D* and *G* modes in graphene and graphite across the visible range has not been experimentally investigated. Such information would be useful while interpreting and validating theoretical work[5,7,10] on the component scattering processes in graphene and graphite that give rise to the *D* mode along with the relevant matrix elements, viz., the electron-phonon coupling and defect scattering. This for instance, has important consequences in determining the phonon dispersion of graphene from Raman experiments. Knowledge of the Raman matrix element $K_{2f,10}$ would also help to determine which laser excitation frequency and underlying substrate configuration gives the most pronounced Raman response.

We measured the Raman spectra of the *D* and *G* modes for graphene and graphite in the visible range and used the method of sample substitution[11] with CaF_2 as a reference to deconvolve the highly wavelength dependent response of the charge-coupled device (CCD) detector and spectrometer optics. In this paper we derive a model that considers graphene suspended on an arbitrary stratified medium while sidestepping its problematic ascription as an object of finite thickness and calculate the absolute Raman response of graphene (and graphite) via its explicitly frequency-independent Raman matrix element squared[3] $|K'_{2f,10}|^2$ as a function of laser frequency. For both graphene and graphite the $|K'_{2f,10}|^2$ per graphene layer vs laser frequency rises rapidly for the *G* mode and less so for the *D* mode across the visible range. We also find a dispersion of the *D* mode position with laser frequency for graphene and graphite of 41 cm^{-1}/eV and 35 cm^{-1}/eV, respectively, in good agreement with Ref. 7. The paper is organized as follows: in Sec. II we derive an expression that relates the experimentally measured Raman spectra to the $|K'_{2f,10}|^2$, Sec. III provides the experimental details of the measurement setup and sample geometry and Sec. IV gives our results and discussion. Finally, Sec. IV is the summary and outlook for our work.

II. THEORY

In this section we derive an expression that relates the experimentally observed photon count R_D as measured by

the spectrometer detector with the quantity of interest, the explicitly frequency-independent Raman matrix element squared $|K'_{2f,10}|^2$ for Sec. II A, an atomically thin graphene layer suspended on a completely general stratified medium and Sec. II B, for the more familiar case of a film of finite thickness relevant for graphite.

A. Raman scattering from a monolayer with an underlying stratified medium

To study Raman scattering in the backscattering configuration we model the graphene sheet as a perfect plane that scatters the incoming laser light of frequency ω_l with an outgoing frequency ω_s. Clearly, the thickness of a monolayer is ill-defined and our approach contrasts previous (although dissimilar) studies on graphene that ascribe a certain thickness to graphene[12] based on atomic force microscopy (AFM) measurements[13] or half the out of plane lattice constant c of Bernal AB graphite $c/2$.

We begin by considering the expression for the Raman matrix element[3,7] $K_{2f,10}$ per graphene layer. We remove all the explicit laser frequency dependencies by factoring out the contribution of the vector potential $\hat{A}$ in the electron-radiation interaction Hamiltonian $\hat{H}_{e-R}=\frac{e}{m_e}\hat{p}.\hat{A}$ which allows $K_{2f,10}$ to be rewritten in terms of the explicitly frequency-independent term $K'_{2f,10}$

$$K_{2f,10}=\frac{e^2\hbar}{2m_e^2\varepsilon_0 L^3\sqrt{\omega_l\omega_s}}e^{i(\mathbf{k_l}-\mathbf{k_s}).\mathbf{r}}K'_{2f,10}. \quad (1)$$

To relate the theoretically accessible Raman matrix element $K_{2f,10}$ to the experimentally obtained D mode Stokes spectra we invoke Fermi's golden rule[14]

$$\frac{\delta w[\omega_s,k_s]}{\delta\Omega}=\frac{2\pi}{\hbar}|K_{2f,10}|^2(N[\hbar\omega_{ph}]+1)\times\rho[\hbar\omega_s-(E_f-E_i),k_s], \quad (2)$$

where $w[\omega_s,k_s]$ is the transition probability per unit time per unit solid angle for the graphene crystal starting from its initial state and reaching a final state with the emission of a photon with energy $\hbar\omega_s$ and wave vector k_s. $N[\hbar\omega_{ph}]$ is the Bose-Einstein factor corresponding to the phonon frequency $\omega_{ph}=\omega_l-\omega_s$. For photons in a fictitious cube of length L we obtain the density of states as $\rho[E_f-E_i-\hbar\omega_s,k_s]=\frac{L^3}{(2\pi)^3}\frac{(\hbar\omega_s)^2}{\hbar^3c^3}$. The differential scattering cross section $\frac{d\sigma}{d\Omega}$ is obtained by dividing $\frac{\delta w[\omega_s,k_s]}{\delta\Omega}$ by the incident photon flux $\Phi=\frac{c}{L^3}$ giving

$$\frac{d\sigma}{d\Omega}=\frac{2\pi}{\hbar}\frac{L^6}{(2\pi)^3}\frac{(\hbar\omega_s)^2}{\hbar^3c^4}\times\frac{e^4\hbar^2}{4m_e^4\varepsilon_0^2L^6\omega_l\omega_s}|K'_{2f,10}|^2(N[\hbar\omega_{ph}]+1), \quad (3)$$

$$=\frac{e^4}{16\pi^2\varepsilon_0^2m_e^4c^4}\frac{\omega_s}{\omega_l}|K'_{2f,10}|^2(N[\hbar\omega_{ph}]+1). \quad (4)$$

The number of photons R reaching the detector per unit solid angle Ω, $\frac{dR}{d\Omega}$ is given by the product of the differential scattering cross section $\frac{d\sigma}{d\Omega}$ and the incident photon flux $\frac{I_l}{\hbar\omega_l}$, where I_l is the laser intensity incident normally on the graphene sheet.

$$\frac{dR}{d\Omega}=\frac{I_l}{\hbar\omega_l}\frac{e^4}{16\pi^2\varepsilon_0^2m_e^4c^4}\frac{\omega_s}{\omega_l}|K'_{2f,10}|^2(N[\hbar\omega_{ph}]+1). \quad (5)$$

If the solid angle subtended by the scattered radiation (and subsequently captured by the microscope objective) is $\Delta\Omega$, the total number of photons R available to the Raman spectrometer over time t shall be

$$R=\frac{I_lt}{\hbar\omega_l}\frac{e^4}{16\pi^2\varepsilon_0^2m_e^4c^4}\frac{\omega_s}{\omega_l}|K'_{2f,10}|^2(N[\hbar\omega_{ph}]+1)\Delta\Omega. \quad (6)$$

The total number of photons registered by the CCD detector R_D inside the Raman spectrometer will be a product of R and the sensitivity $S[\omega]$ of the entire spectrometer optics including the response characteristics of its CCD detector which we assume to be a function of only the scattering/incident frequency. Here we also make the assumption that the two frequencies are close enough such that $\omega_l\simeq\omega_s$ or equivalently that $S[\omega]$ varies insignificantly over the relative Raman frequencies of interest.

$$R_D=S[\omega]R=S[\omega]\frac{I_lt}{\hbar\omega_l}\frac{e^4}{16\pi^2\varepsilon_0^2m_e^4c^4}\times\frac{\omega_s}{\omega_l}|K'_{2f,10}|^2(N[\hbar\omega_{ph}]+1)\Delta\Omega. \quad (7)$$

The sensitivity function $S[\omega]$ corresponding to each Raman spectrometer setup is obtained using the method of sample substitution.[11] In this method we perform Raman measurements on a reference sample with experimental conditions that are identical to those prevailing for the material whose absolute Raman response is sought. The reference crystal is a large band gap material of very low dispersion for which the Raman tensor is known.[15] We employed the (111) surface of CaF_2 for which the Raman tensor component $|a|=0.47$ A^2 is known experimentally for the 322 cm^{-1} Raman peak and is constant in the visible range.[16]

We locate the plane containing the graphene sheet at a distance L equal to the graphene "thickness" as measured by AFM $z_d=0.335$ nm (Ref. 13) (and which is also $c/2=0.335$ nm for graphite) away from the SiO_2-ambient interface. To account for the effect of the underlying substrate on the $K_{2f,10}$ of bare graphene we consider the scattering plane in the limit of an electric dipole. This is fully consistent with the usually employed equivalent form of the light-matter interaction Hamiltonian, the dipole approximation.[14] In the dipole approximation the light-matter interaction Hamiltonian $H'_{e\text{-}R}=-\hat{d}.\hat{E}_\perp[0]$, where $\hat{d}$ is the dipole moment operator and $\hat{E}_\perp[0]$ is the electric field operator incident on the sample. It holds when the lattice constant of the material is much smaller than the probing wavelength. The underlying substrate affects the inelastically scattered radiation from the scattering plane (in the far-field approximation, i.e., the detector is far from the emitting dipole) via an enhancement factor $F[z_d]$. z_d is the location of the graphene sheet,[17,18] z_1

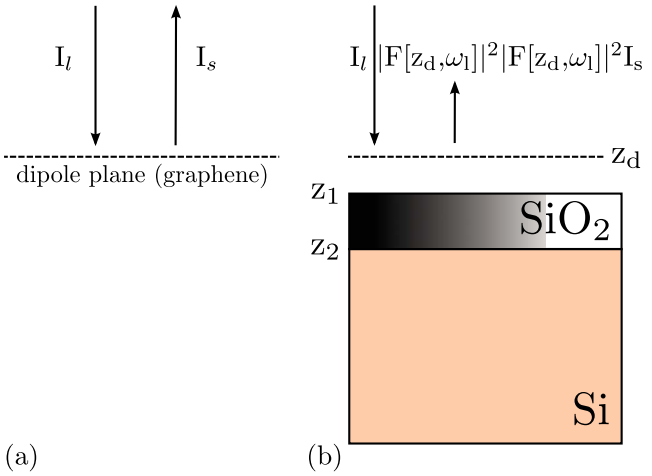

FIG. 1. (Color online) The model dipole layer (graphene) located at position z_d is taken to be 0.335 nm above the ambient-SiO_2 interface denoted by z_1. The Si-SiO_2 is denoted by z_2. The contribution of the total enhancement factor $|F[z_d,\omega_l]|^2|F[z_d,\omega_s]|^2$ is illustrated while comparing the configurations (a) bare graphene and (b) graphene suspended over the SiO_2-Si strata.

denotes the ambient-SiO_2 interface and z_2 the SiO_2-Si interface (see Fig. 1). $F[z_d]$ may be understood as the ratio of the emitted electric field of the dipole with and without the presence of the underlying stratified medium.[18] For the stratified medium under our experimental consideration: the ambient-SiO_2-Si stack, the enhancement factor is [see Eq. (8) of Ref. 18 for $z>z_1$]

$$F[z,\omega] = 1 + r_\perp[\omega]e^{2i(\omega/c)(z-z_1)}, \tag{8}$$

where $r_\perp$ is the reflection coefficient of the ambient-SiO_2-Si interface which can be calculated by the standard transfer-matrix formalism.[19] The enhancement factor comes into play once for the light-matter interaction matrix element corresponding to the excitement of the electron-hole pair as $F[z_d,\omega_l]$ and subsequently for the matrix element corresponding to the electron-hole de-excitation as $F[z_d,\omega_s]$. This leads to an overall multiplicative contribution of $|F[z_d,\omega_s]|^2|F[z_d,\omega_l]|^2$ to the backscattered intensity of the monolayer due to the presence of the substrate. This is valid for a completely arbitrary underlying stratified medium; all the information about the substrate is contained in its reflection coefficient $r_\perp$. We may express the incident intensity $I_l = P_l/A$ where P_l is the incident power and A is the area of the Gaussian laser spot. Finally, the counts registered by the CCD detector for the scattering plane in the presence of the underlying medium become:

$$R_D^{graphene} = |F[z_d,\omega_l]|^2|F[z_d,\omega_s]|^2 S[\omega]\frac{P_l t}{A\hbar\omega_l} \times \frac{e^4}{16\pi^2\varepsilon_0^2 m_e^4 c^4}\frac{\omega_s}{\omega_l}|K'_{2f,10}|^2(N[\hbar\omega_{ph}]+1)\Delta\Omega_{graphene}. \tag{9}$$

B. Raman scattering from films with a finite thickness

For samples with finite thickness such as CaF_2 and graphite, the backscattered intensity I_b can be written in terms of the incident intensity I_0 and native scattering efficiency ξ of the material as[20]

$$I_b = I_0\frac{1-e^{-(\xi+\alpha_l+\alpha_s)L}}{\xi+\alpha_l+\alpha_s}T_l[\omega_l]T_s[\omega_s], \tag{10}$$

where α_l and α_s are the absorption coefficients corresponding to the incoming and outgoing radiation, $T_l[\omega_l]$ and $T_s[\omega_s]$ are the transmittances of the incoming radiation from the ambient into the sample and from the sample into the ambient, respectively. The transmittances can be calculated from the transfer-matrix method. The expression for I_b in Eq. (10) can be simplified considerably in the regimes of highly transparent and highly absorbing samples. For a highly absorbing sample (for e.g., graphite) we obtain

$$I_{b,absorbing} = \frac{I_0\xi}{\alpha_l+\alpha_s}T_l[\omega_l]T_s[\omega_s] \tag{11}$$

whereas for highly transparent samples (for e.g., CaF_2)

$$I_{b,transparent} = I_0\xi L T_l[\omega_l]T_s[\omega_s], \tag{12}$$

where L is the sample length in the z direction or the depth of focus of the microscope objective, whichever is smaller. The relevant expression for graphite now becomes

$$R_D^{graphite} = S[\omega]\frac{I_l t}{\hbar\omega_l}\frac{e^4}{16\pi^2\varepsilon_0^2 m_e^4 c^4}\frac{\omega_s}{\omega_l}|K'_{2f,10}|^2 \times [N(\hbar\omega_{ph})+1]T_l[\omega_l]T_s[\omega_s]\Delta\Omega_{graphite}\left[\frac{2}{c(\alpha_l+\alpha_s)}\right]. \tag{13}$$

Note that the factor $\frac{2}{c(\alpha_l+\alpha_s)}$ accounts for the number of graphene layers over an *effective* scattering length $L_{eff} = \frac{1}{\alpha_l+\alpha_s}$ of the graphite sample. For films of finite thickness such as for the reference crystal CaF_2 (where the concept of a primitive unit volume V_c is meaningful) it is convenient to work with an equivalent expression instead of Eq. (13) since the tabulated values of the absolute Raman response are commonly available in the literature in terms of the Raman tensor component $|a|$, giving us, for example, for CaF_2 (Ref. 21)

$$R_D^{CaF_2} = S[\omega]P_l t L\frac{\omega_s^3 n_{CaF_2}[\omega_s]}{c^4 2V_C M_r\omega_{ph}n_{CaF_2}[\omega_l]} \times T_l[\omega_l]T_s[\omega_s]a^2_{CaF_2}(N[\omega_{ph}]+1)\Delta\Omega_{CaF_2}, \tag{14}$$

where M_r is the reduced mass of the vibrating atoms inside the primitive unit cell of volume V_c and ω_{ph} is the measured phonon frequency.

III. EXPERIMENTAL DETAILS

A. Graphene

A flake of graphene, prepared by micromechanical exfoliation, was suspended on an Si substrate overlaid with a

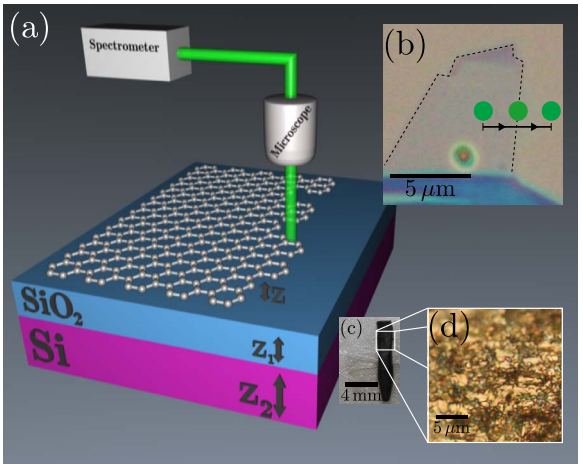

FIG. 2. (Color online) (a) Experimental configuration for measuring the D mode at the graphene edge which is located at a distance z above the ambient-SiO_2 interface located at z_1. z_2 locates the Si-SiO_2 interface. The SiO_2 layer thickness is (293.7 ± 0.5) nm while the Si layer is assumed semi-infinite. (b) Optical image of the graphene flake under consideration. The laser spot was scanned along the line indicated. (c) The pencil lead upon which the measurement for graphite was carried out. (d) Microstructure of pencil graphite observed under 100× optical magnification indicating a highly defected structure.

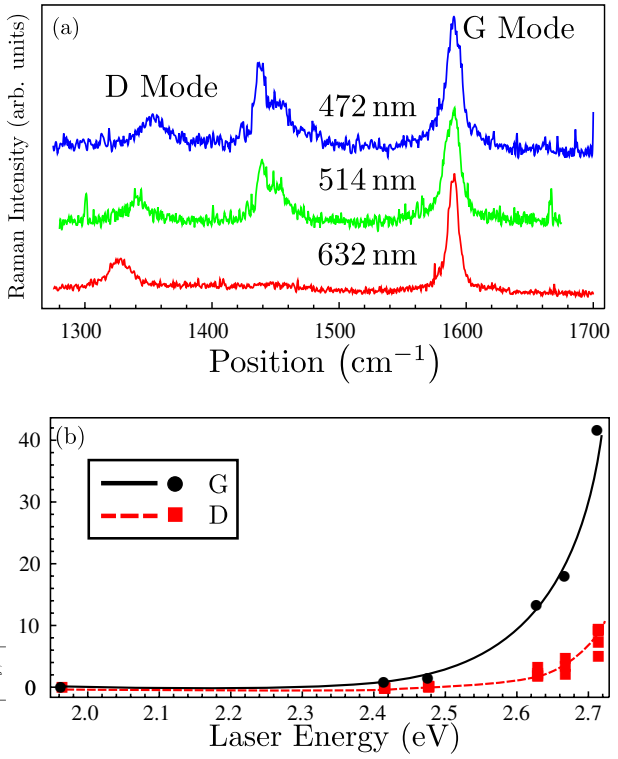

FIG. 3. (Color online) (a) Representative Raman spectra of graphene obtained for laser excitation wavelengths 632 nm (red), 514 nm (green), and 472 nm (blue). (b) $|K'_{2f,10}|^2$ for the graphene monolayer vs laser energy (eV) for the G (black circles) and D modes (red squares). The corresponding lines are a guide to the eye.

thermally grown (293.7 ± 0.5) nm [as measured by a Sentech SE801 ellipsometer using a deuterium/halogen lamp (AvaLight-DHS-Bal)] SiO_2 layer (see Fig. 2). At room temperature ~295 K it was subject to a range of visible-range laser excitation and analyzed in the micro mode with a T64000 Jobin-Yvon Raman spectrometer with a Nikon MPlan 100× microscope objective. Although graphene prepared by mechanical exfoliation contains defects, their density is typically too low to give an appreciable D mode signal without exceedingly long exposure times or alternately power levels that may lead to heating effects.[9] We scanned the laser spot perpendicularly across the graphene edge [see Fig. 2(b)] which serves as an identifiable and repeatable defect that breaks the translational symmetry of the two-dimensional crystal structure of graphene. The electric field polarization of the laser was chosen to be parallel to the edge direction which is known to give the maximal Raman response of the D mode.[10] In order to expose nominally the same number of defect sites for every laser excitation wavelength we aim the spot such that it is incident half on graphene and half outside it [see Fig. 2(b)]. This configuration has also been shown to produce the maximum D mode signal.[10] The total integrated laser power at all times was maintained at a level below 0.4 mW over a laser spot size on the order of 0.5 μm radius to preclude any heating effects in the graphene flake.[9]

B. Graphite

Due to the very short depth-of-field of the high-magnification optical microscope objective (~1 μm), repeatably isolating a perfect edge proved difficult due to the presence of irregular ledges and overhangs in a highly oriented pyrolitic graphite highly oriented pyrolytic graphite (HOPG) flake. We therefore decided to average over a larger sample area, employing instead the macromode of the spectrometer that features a laser spot size that is about 30 times larger in diameter compared to the micromode and a depth of focus that exceeds a few millimeters. Yet even across this augmented area the bulk region of the HOPG still gave a very low D mode signal indicating a very low density of defects in our sample and which are frequently deemed absent for high-quality HOPG samples.[22] In order to observe an appreciable D mode signal we finally settled on a humble graphite pencil lead [see Fig. 2(c)] which consists of grains of highly defected graphite bonded to a bentonite clay matrix.

IV. RESULTS AND DISCUSSION

A. Graphene

For graphene we found a D mode dispersion of 41 cm^{-1}/eV which is in excellent agreement with our previous calculations[7] and yet further confirms the validity of the double-resonant approach in determining the D mode. The experimentally determined $|K'_{2f,10}|^2$ for the D and G modes of graphene are shown in Fig. 3(b). For the D mode the $|K'_{2f,10}|^2$ values account for the fact that they are observed with the laser spot center imprecisely at the graphene edge line. By measuring the G mode in a location far-away from

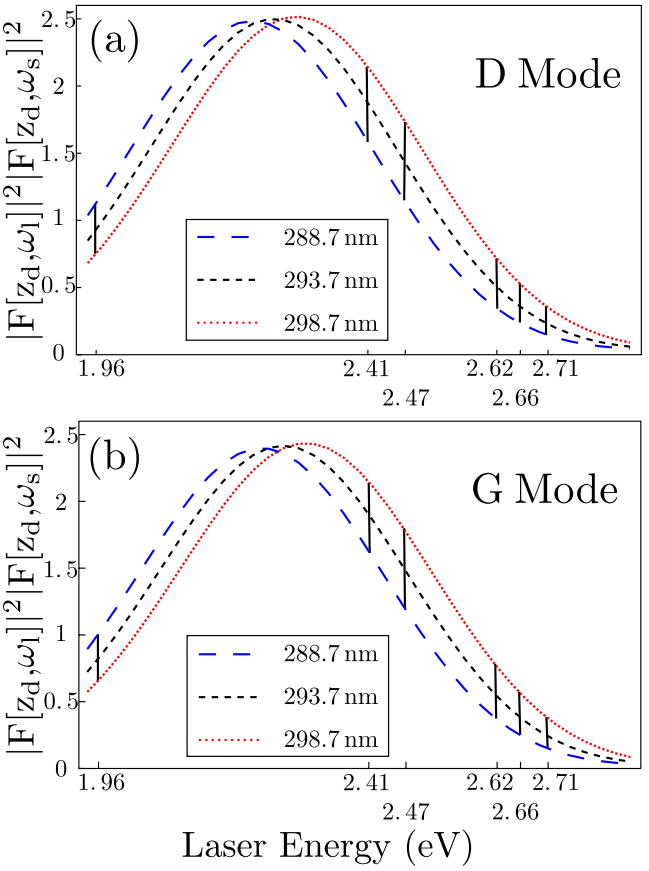

FIG. 4. (Color online) Variation in the total enhancement factor of Eq. (8), $|F[z_d,\omega_s]|^2|F[z_d,\omega_l]|^2$ for graphene suspended on a SiO_2-Si layer as a function of laser energy for a (293.7 ± 0.5) nm variation in SiO_2 thickness for (a) the D mode and (b) the G mode. The solid black lines indicate the variation in the total enhancement factor $|F[z_d,\omega_s]|^2|F[z_d,\omega_l]|^2$ for the incident laser energies employed.

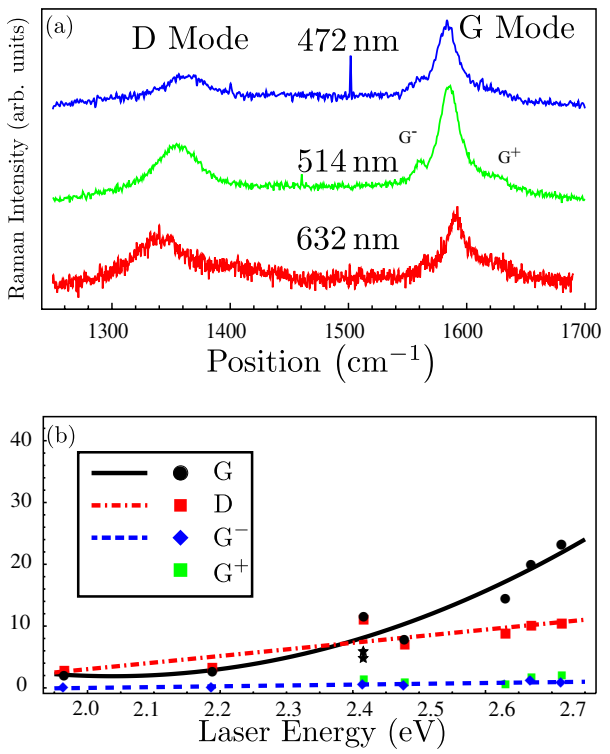

FIG. 5. (Color online) (a) Representative Raman spectra of graphite obtained for laser excitation wavelengths 632 nm (red), 514 nm (green), and 472 nm (blue) with indicated D, G, G^-, and G^+ modes. (b) $|K'_{2f,10}|^2$ for graphite per unit area per graphene layer vs laser energy (eV) for the G (solid black circles), D (red squares), G^- (blue diamonds), and the G^+ modes (green squares). The corresponding lines are a guide to the eye.

the edge a correction can be applied as described by Casiraghi *et al.*[10] who obtained the D mode at a graphene edge using a piezoelectrically controlled stage. The relative intensity of the D mode achieves a maximum at the edge location whereas the G mode is nominally half its strength at the edge compared to its bulk value.[10] It is important to keep in mind that the incident intensity employed in the calculation for the D mode $|K'_{2f,10}|^2$ is twice the intensity prevailing experimentally. This is because in order to obtain the maximum D mode the graphene sheet only receives half the laser footprint and therefore only half its intensity.

The origin of the increasing D and G mode $|K'_{2f,10}|^2$ with laser energy may be due to the approaching Van Hove singularity (and the concomitant increase in the density of states) at the M point of the electronic dispersion of graphene. Since the visible range of laser energies lie on the shoulder of this Van Hove singularity, our results for the intensity of the D mode in Ref. 7 were deemed constant on the scale presented. However, on rescaling our results we again find a nearly linearly increasing D mode in good agreement with the experimentally observed intensity profile.

Our calculation for the $|K'_{2f,10}|^2$ of graphene assumes a total enhancement factor $|F[z_d,\omega_s]|^2|F[z_d,\omega_l]|^2$ which is calculated for an SiO_2 thickness of (293.7 ± 0.5) nm and changes quite rapidly even with a ±5 nm variation (see Fig. 4) which needs to be reckoned with for an imperfectly flat sheet of graphene which may be due to the intrinsic ripples in graphene[23] or sandwiched molecules (e.g., H_2O) between the graphene layer and the SiO_2 layer. Therefore, our results should be interpreted with care, giving due consideration to their variation as indicated by the vertical solid black lines of Figs. 4(a) and 4(b) for the D and G modes, respectively.

A comparison with previously published data on graphite[24] and standard scatterers such as diamond[11,25] and silicon[24,26] in terms of the conventionally quoted Raman tensor component $|a|$ values based on Eq. (14) is given in Table I together with their absorption coefficients $\alpha_{l,s}$ as material parameters. The value of $|a|$ for graphene is obtained by using the volume of its unit cell $V_{c,graphene}=0.5\times V_{c,graphite}$, reduced mass $M_{r,graphene}=2\times M_{r,graphite}$, and scattering length $L=z_d=0.335$ nm. The transmission coefficients $T_{l,s}$ are obtained using the transfer matrix formalism for the ambient-graphene-SiO_2-Si stack with L as the assumed graphene thickness.

B. Graphite

The explicitly frequency independent Raman matrix element squared $|K'_{2f,10}|^2$ per unit area per graphene layer for the

TABLE I. A comparison of the Raman tensor component $|a|$ and material parameters for various materials at the 514.5 nm laser wavelength.

Material	Phonon symmetry, wave number (cm^{-1})	α_l (m^{-1})	α_s (m^{-1})	Ref.	$\|a\|$ (A^2)	Ref.
Diamond	F_{2g}, 1332	0	0	28	4.4	11
					3.9	25
Silicon	F_{2g}, 525	1×10^6	0.75×10^6	29	66	24
					77	26
Graphite	E_{2g}, 1585 (G mode)	3.72×10^7	3.41×10^7	30	88	24
		4.18×10^7	3.84×10^7	31	104	24
		3.35×10^7	3.16×10^7	30	131	This work
	A_1', 1355 (D mode)	3.35×10^7	3.18×10^7	30	118	This work
Graphene	E_{2g}, 1584 (G mode)	3.35×10^7	3.16×10^7	30	92	This work
	A_1', 1343 (D mode)	3.35×10^7	3.18×10^7	30	69	This work

G and D modes for graphite are given in Fig. 5(b). The G mode $|K'_{2f,10}|^2$ increases rapidly with increasing laser energy as indicated by the black line of Fig. 5(b). We observe a good agreement with previous experimental results of Wada and Solin[24] for the (albeit single) 514.5 nm excitation frequency [see the black starred points in Fig. 5(b)] calculated from the Raman tensor component $|a|$ for the G mode of HOPG. Also given are the results for the G^- and G^+ modes that can be discerned in our spectra at 1559 and 1624 cm^{-1} for the 514.5 nm laser line, for instance [see Fig. 5(a)]. Our results show a steady, nearly linearly increasing D mode $|K'_{2f,10}|^2$. The observed rise of the D and G modes with increasing laser frequency may be explained identically to the case of graphene discussed earlier.

A dispersion of the D mode position with laser energy of 35 cm^{-1}/eV was found which is slightly lower than previously reported values on HOPG [44–51 cm^{-1}/eV (Refs. 27, 32, and 33)] and may be due to the smaller grain size of the microcrystallites present in pencil graphite but nevertheless agrees well with our theoretical prediction based on constant matrix elements.[7]

V. SUMMARY AND OUTLOOK

We have measured the Raman spectra of graphene and graphite for the D and G modes across the visible range of laser energies. The absolute Raman response of the bare material under consideration was obtained using the method of sample substitution[11] with CaF_2 as a reference[16] that allows the deconvolution of the highly wavelength-dependent response of the spectrometer optics and its CCD detector. The effect of the underlying stratified medium on the Raman response of graphene, via electromagnetic enhancement was modeled by considering the scatterer in the limit of an electric dipole. We derived an expression that relates the experimentally measurable spectra to the absolute Raman response of the bare material as encoded by the explicitly frequency-independent Raman matrix element squared $|K'_{2f,10}|^2$ per unit area per graphene layer considering graphene in the paradigm of a perfect plane scatterer, thus avoiding the problematic ascription of a thickness value for graphene. Our model was further extended to the more familiar case of a scatterer of finite thickness, e.g., graphite.

Our results showed that the $|K'_{2f,10}|^2$ per graphene layer vs laser energy rises rapidly for the G mode and less so for the D mode (see Figs. 3 and 5). This may be due to the approaching Van Hove singularity of the M points in the electronic dispersions of both graphene and graphite. The D mode dispersion for graphene was 41 cm^{-1}/eV in excellent agreement with our earlier theoretical prediction.[7] Whereas a dispersion of 35 cm^{-1}/eV was found for pencil graphite which is somewhat lower than the reported values of HOPG of 44–51 cm^{-1}/eV.[27,32–35] Our results shall aid in the experimental verification of the electron-phonon, electron-defect scattering matrix elements in the visible range of the energy scale that may be obtained using theoretical or *ab initio* methods and shall be the subject of a future publication.

ACKNOWLEDGMENTS

We thank Christoph Cobet and Norbert Esser from the Leibniz-Institut für Analytische Wissenschaften - ISAS - e.V. for aiding with the ellipsometric measurement. This work was supported by ERC under Grant No. 210642-OptNano.

[1] K. S. Novoselov, A. K. Geim, S. V. Morozov, D. Jiang, Y. Zhang, S. V. Dubonos, I. V. Grigorieva, and A. A. Firsov, Science **306**, 666 (2004).
[2] A. K. Geim and K. S. Novoselov, Nature Mater. **6**, 183 (2007).
[3] L. M. Falicov and R. M. Martin, *Light Scattering in Solids I: Introductory Concepts, chapter Resonant Raman Scattering* (Springer-Verlag, Berlin, 1983), p. 83.
[4] Not to be confused with the usual definition of the matrix element: $\langle\psi_f|\hat{H}|\psi_i\rangle$.
[5] C. Thomsen and S. Reich, Phys. Rev. Lett. **85**, 5214 (2000).
[6] S. Reich and C. Thomsen, Philos. Trans. R. Soc. London **362**, 2271 (2004).
[7] R. Narula and S. Reich, Phys. Rev. B **78**, 165422 (2008).
[8] M. Burghard, Surf. Sci. Rep. **58**, 1 (2005).
[9] A. C. Ferrari, J. C. Meyer, V. Scardaci, C. Casiraghi, M. Lazzeri, F. Mauri, S. Piscanec, D. Jiang, K. S. Novoselov, S. Roth, and A. K. Geim, Phys. Rev. Lett. **97**, 187401 (2006).
[10] C. Casiraghi, A. Hartschuh, H. Qian, S. Piscanec, C. Georgi, A. Fasoli, K. S. Novoselov, D. M. Basko, and A. C. Ferrari, Nano Lett. **9**, 1433 (2009).
[11] M. Grimsditch, M. Cardona, J. M. Calleja, and F. Meseguer, J. Raman Spectrosc. **10**, 77 (1981).
[12] D. Yoon, H. Moon, Y.-W. Son, J. S. Choi, B. H. Park, Y. H. Cha, Y. D. Kim, and H. Cheong, Phys. Rev. B **80**, 125422 (2009).
[13] A. Gupta, G. Chen, P. Joshi, S. Tadigadapa, and Eklund, Nano Lett. **6**, 2667 (2006).
[14] G. Grynberg, C. Cohen-Tannoudji, and J. Dupont-Roc, *Atom-Phonon Interactions: Basic Processes and Applications* (Wiley, New York, 1992).
[15] M. Cardona, *Light Scattering in Solids II* (Springer-Verlag, Berlin, 1982).
[16] J. M. Calleja, H. Vogt, and M. Cardona, Philos. Mag. A **45**, 239 (1982).
[17] Jin Au Kong, *Electromagnetic Wave Theory* (Wiley, New York, 1986).
[18] O. H. Crawford, J. Chem. Phys. **89**, 6017 (1988).
[19] M. Born and E. Wolf, *Principles of Optics* (Cambridge University Press, Cambridge, 1999).
[20] R. Loudon, J. Phys. (France) **26**, 677 (1965).
[21] C. Trallero-Giner, A. Cantarero, M. Cardona, and M. Mora, Phys. Rev. B **45**, 6601 (1992).
[22] D. B. Fischbach and M. Couzi, Carbon **24**, 365 (1986).
[23] J. C. Meyer, A. K. Geim, M. I. Katsnelson, K. S. Novoselov, T. J. Booth, and S. Roth, Nature (London) **446**, 60 (2007).
[24] N. Wada and S. A. Solin, Physica B & C **105**, 353 (1981).
[25] E. Anastassakis and E. Burstein, Phys. Rev. B **2**, 1952 (1970).
[26] M. Cardona and M. Grimsditch, Proceedings of the 14th International Conference on the Physics of Semiconductors Edinburgh, Scotland, 1978 (unpublished), p. 639.
[27] I. Pócsik, M. Hundhausen, M. Koos, and L. Ley, J. Non-Cryst. Solids **227-230**, 1083 (1998).
[28] The absorption of diamond at 514.5 nm is assumed negligible.
[29] T. P. McLean, Prog. Semicond. **5**, 53 (1960).
[30] E. A. Taft and H. R. Philipp, Phys. Rev. **138**, A197 (1965).
[31] J. Daniels, C. v. Festenberg, H. Raether, and K. Zeppenfeld, Springer Tracts Mod. Phys. **54**, 77 (1970).
[32] M. J. Matthews, M. A. Pimenta, G. Dresselhaus, M. S. Dresselhaus, and M. Endo, Phys. Rev. B **59**, R6585 (1999).
[33] Y. Wang, D. C. Alsmeyer, and R. L. McCreery, Chem. Mater. **2**, 557 (1990).
[34] S. Latil, V. Meunier, and L. Henrard, Phys. Rev. B **76**, 201402 (2007).
[35] H. S. Wong and C. Durkan, Phys. Rev. B **81**, 045403 (2010).